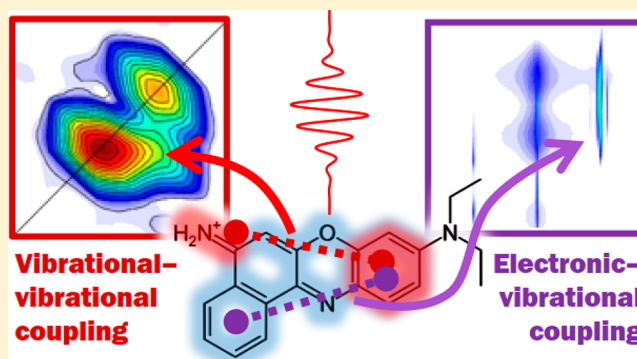


Four-Dimensional Coherent Spectroscopy of Complex Molecular Systems in Solution

Austin P. Spencer,¹ William O. Hutson, and Elad Harel*¹

Department of Chemistry, Northwestern University, Evanston, Illinois 60208, United States

ABSTRACT: An understanding of microscopic interactions in solution is of fundamental importance in chemistry. However, the structure and dynamics of complex systems in the condensed phase, especially far from thermal equilibrium, are masked by broad and often featureless absorption and emission spectra. Nonlinear optical spectroscopy has proven to be a powerful and general approach to disentangling congested spectra by spreading information across multiple dimensions, revealing features oftentimes hidden in lower-order projections. As the dimensionality of the measurement is increased, the better the microscopic interactions are revealed, as spectral bands disperse in the large hyper-spectral volume. This capability, however, comes at a steep price, as the signal decreases exponentially at higher orders of optical response, and added experimental complexity increases noise. We discuss a 4D coherent spectroscopy known as gradient-assisted multidimensional electronic–Raman spectroscopy (GAMERS) that reveals coupling between electronic and vibrational transitions in complex, condensed-phase systems ranging from organic molecules to semiconductor nanocrystals. We reveal that high-resolution spectra may be extracted from these systems even in the presence of severe spectral broadening, both homogeneous and inhomogeneous in origin. The theoretical and experimental underpinnings of this method are discussed. Increasingly, higher-order and higher-dimensionality spectroscopies like GAMERS are needed to understand the microscopic interactions that connect structure to dynamics to function.



1. INTRODUCTION

It is becoming increasingly evident through extensive experimental and theoretical efforts that the coupling between and among electronic and vibrational degrees of freedom may dictate the structure and dynamics of many complex chemical systems. Correlations among vibronic states, for instance, may control the efficiency of energy- and charge-transfer processes in a photosynthetic antenna,¹ rates of singlet fission in certain organic films,² and the rate of carrier cooling in semiconductor nanocrystals³ (via vibrational modes of the ligand molecules or phonon modes associated with the surface). However, revealing these correlations by traditional ensemble spectroscopic approaches is generally challenging because of severe spectral congestion and the presence of inhomogeneous broadening. The idea to measure correlations between different quantum states using multidimensional nuclear magnetic resonance (NMR) spectroscopy has found enormous success for elucidating both the structure and the dynamics of complex spin systems, which has led to important breakthroughs in chemical physics, structural biology, and materials science.^{4–6} Three decades after Jeener first proposed 2D NMR,⁷ the optical analog, 2D electronic spectroscopy (ES), has proliferated as a powerful approach to study the electronic and vibrational structure and the dynamics of complex, condensed-phase systems with femtosecond resolution. 2D ES, also known as 2D photon-echo spectroscopy, has been used to examine the dynamics of energy transfer in photosynthetic proteins,^{8–10}

ultrafast dynamics of solute–solvent species,¹¹ intraband relaxation in semiconductors,^{12,13} singlet fission in polyacenes,¹⁴ and dynamics in proteins,¹⁵ to name a few applications.

However, whereas 2D ES and 2D infrared (IR) spectroscopy are powerful methods in their own right, as with 2D NMR, their limitations become apparent as the complexity of the system increases. For instance, the ability to assign the origin of quantum coherent beating signals in photosynthetic pigment–protein complexes to either ground or electronically excited states has proven to be limited by the information available in the 2D ES measurement.^{16–18} Spectral congestion coupled to homogeneous and inhomogeneous broadening, fast dynamics, and a multitude of possible coherence pathways makes the assignment of signals extremely challenging. In 2D IR,¹⁹ the system is always confined to the ground state, but limited spectral bandwidth of IR sources makes it challenging to probe the entire fingerprint region (1000–4000 cm⁻¹) or low-frequency regions below ~500 cm⁻¹. Raman spectroscopy could, in principle, overcome both of these limitations, but despite tremendous efforts over two decades,^{20–22} early nonresonant 2D Raman experiments were dominated by lower-order cascaded signals and not the true fifth-order signals

Received: September 19, 2018

Revised: November 18, 2018

Published: November 30, 2018

that give unique information on vibrational coupling, which is vital for studying the structure and dynamics of liquids.

These limitations have motivated the exploration of higher-order and higher-dimensionality coherent spectroscopies,^{23–25} but, as with the case of NMR, long acquisition times hinder the practical implementation of these methods. In fact, the situation is actually significantly worse in the optical regime because the pulses quickly lose their phase correlation,²⁶ a situation that becomes exacerbated with an increasing number of pulses. Even more problematic is the weak signals resulting from the nonlinear optical response, which decrease exponentially at higher order and with the addition of more pulses. This is in contrast with the case of NMR, where the signal strength is relatively constant irrespective of the number of pulses because nearly all (>99%, typically) of the spins interact with each pulse, and the interactions are in the strong-pulse (i.e., non-perturbative) limit. The weak optical signals create the need to increase the pump fluence, which leads to faster sample photodamage, thereby limiting acquisition times of the multiple temporal dimensions. Another major issue is that in ES the excited-state population dynamics overwhelm the much weaker coherences, making it difficult to extract information about the vibronic frequencies and their amplitude, a situation that does not exist in NMR, where only coherences are measured. Other issues include the need to perform background-free measurements (because the $|\chi^{(5)}|^2$ signal may be $<10^{-8}$ of the pump intensity), competition from lower-order signals (e.g., $\chi^{(5)} < 10^{-3}\chi^{(3)}$), the need to keep all n pulses overlapped in time and space over the measurement period, additive and multiplicative noise sources, and so on. In NMR, the pulses are phase-stable indefinitely for all intents and purposes, the wavelength is much longer than the sample dimensions, so there are no spatial coherence or pulse overlap issues, and phase cycling easily isolates the desired coherence pathway.

Recently, the authors reported²⁷ a new experimental approach for accessing vibrational–vibrational coupling information with electronic-state specificity without contamination from low-order cascades using a method called Gradient-Assisted Multidimensional Electronic–Raman Spectroscopy (GAMERS). This method extends 2D ES by introducing an additional nonresonant prepump pulse prior to the typical three-pulse sequence that selectively excites ground-state vibrational coherences through Raman pathways. The additional vibrational dimension allows for measuring correlations with the resonantly excited coherences generated during the subsequent population time of the 2D ES pulse sequence. Critically, the use of a nonresonant prepump ensures that the coherences observed during the first time period are dominated by ground-state vibrations, providing a reference for comparison to frequencies measured during later time periods to isolate the excited-state pathways.

GAMERS has been applied to a variety of chemical systems, ranging in complexity from organic dyes^{27,28} to quantum dots (QDs).²⁹ It has been demonstrated that GAMERS spectrally isolates distinct coherence pathways by dispersing the signal across as many as four frequency dimensions, yielding specificity that is not possible in 2D ES. In cadmium selenide (CdSe) QDs, a 3D version of GAMERS revealed excitonic-state-dependent coupling to longitudinal optical (LO) and acoustic phonon modes.²⁹ Despite measuring a room-temperature sample with considerable polydispersity, the GAMERS spectra revealed a frequency shift between LO phonon modes coupled to different

excitonic transitions that was significantly less than the phonon line width.

Whereas GAMERS has considerably more information content than 2D ES, it comes at the price of reduced signal strength and substantially longer acquisition times to sample all of the coherence dimensions. Significant advances have been made in reducing the acquisition time required to measure a 4D GAMER spectrum using spatial multiplexing methods. We have demonstrated²⁷ the advantage of spatially encoding pulse time delays in the sample as in GRAdient-Assisted Photon-Echo Spectroscopy (GRAPES),³⁰ which is necessary to make this experiment feasible because it reduces the time needed to acquire a spectrum with n^4 points by a factor of n . In addition, we established³¹ that radially sampling the (T_0, T) plane further reduces the acquisition time by approximately an order of magnitude, with no appreciable loss in resolution. In this method, slices acquired at various angles through the origin of the (T_0, T) plane are used to reconstruct the 4D GAMER spectrum using the inverse Radon transform (e.g., back-projection algorithm). Novel reconstruction methods that extend beyond the Fourier transform have yielded spectra with a dynamic range on the order of 10^4 ; this is at least two orders of magnitude larger than in corresponding third-order experiments and is a key requirement for observing small signals that are suppressed by the weak optical response. We demonstrate that the increased spectral resolution and ultrahigh sensitivity allow for high-resolution spectroscopy of complex condensed-phase systems.

First, we describe the GAMERS technique from the standpoint of methodology, theory, and analysis. We will summarize the subsequent development and improvement of GAMERS as well as some of the significant discoveries in organic dyes and QDs. Finally, we will present new results using state-of-the-art acquisition and processing methods that highlight the high spectral resolution and dynamic range afforded by 4D GAMERS as well as discuss future directions for elucidating the structure and dynamics of complex chemical systems.

2. GAMERS THEORY

As shown in Figure 1a, the pulse sequence for GAMERS is identical to the three-pulse sequence of 2D ES, except that a prepulse is used to prepare the system in a coherence at the ground state rather than an equilibrated population state determined by the system temperature. This prepulse is nonresonant with the $S_0 \rightarrow S_1$ transition of the molecule so that a nonequilibrium initial state is prepared by means of impulsive Raman scattering for subsequent resonant 2D ES. After each pulse in the sequence, either a population or coherence is formed depending on whether the interaction with the field occurs with the bra or ket of the density matrix. Populations are formally diagonal elements of the density matrix of the form $|a\rangle\langle a|$, whereas coherences are given by the off-diagonal elements $|a\rangle\langle b|$, where $a \neq b$. When the states $|a\rangle$ and $|b\rangle$ correspond to the same electronic state, their coherence is termed a zero-quantum coherence (ZQC). When the states possess different excitation quanta, they are categorized as single-quantum coherences (SQCs), double-quantum coherences (DQCs), and so on. Traditional 2D ES examines the correlation between SQCs corresponding to absorption and stimulated emission (or photoinduced absorption) as a function of the waiting time T between the second and third pulses. However, the waiting time period may also encode ZQCs, which are the beating-type signals that have been observed in a wide

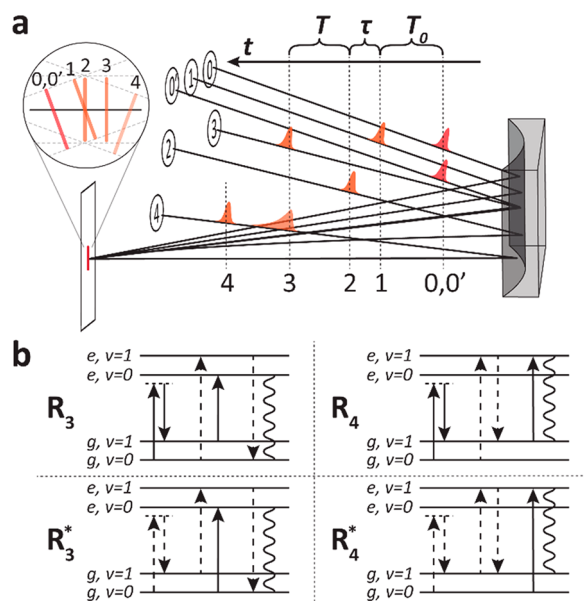


Figure 1. Overview of the GAMERS experiment. (a) Cartoon of the background-free GAMERS apparatus showing the five excitation pulses (0, 0', 1, 2, 3) and local oscillator (4) focused by a cylindrical mirror in the sample, along which the τ delay is spatially encoded. (b) Energy ladder diagrams describe the possible coherence pathways accessible by GAMERS. In the context of the density matrix, dashed and solid arrows represent changes to the state of the bra and ket, respectively, with the final wavy line denoting radiation of the signal.

variety of systems from photosynthetic protein complexes³² to QDs.³³ In the case of GAMERS, the initial excitation creates an additional ZQC on the ground electronic state, so that in all, the 4D spectrum maps electronic–electronic (2D SQC), vibrational–vibrational (2D ZQC), and electronic–vibrational (2D SQC–ZQC) interactions. Therefore, the 4D GAMER spectrum $\hat{S}(\omega_{T_0}, \omega_\tau, \omega_T, \omega_t)$ is composed of two “Raman-like” ZQC dimensions (ω_{T_0} and ω_T) that resolve vibrational and low-frequency electronic coherences and two “optical” SQC dimensions (ω_τ and ω_ν known as the excitation and detection dimensions, respectively) that resolve high-frequency electronic coherences. As a fully coherent method, the spectrum reveals couplings between transitions along all four dimensions.

Because a 4D spectrum is challenging to visualize, 2D slices and projections are often helpful for interpreting the information content of the GAMER spectrum. For example, at each point in the (ω_τ, ω_t) plane, one can extract a 2D Raman-like spectrum containing the vibrational modes that couple to the electronic transition at the chosen (ω_τ, ω_t) point. Known as 2D Raman spectra, or 2D beating slice (2DBS) spectra,²⁷ they contain information regarding the coupling between the various nuclear modes, such as through anharmonicity or vibrational relaxation. Similarly, at each point in the (ω_{T_0}, ω_T) plane, one can extract a 2D beating map (2DBM) spectrum²⁷ that reveals which electronic transitions couple to the vibrational mode at the chosen (ω_{T_0}, ω_T) point. In addition to these purely electronic or vibrational slices, there are also mixed electronic–vibrational slices in which the 6WM signal is displayed as a function of one electronic dimension (ω_τ or ω_t) and one vibrational dimension (ω_{T_0} or ω_T). These slices are particularly useful for highlighting differences in vibrational frequencies between different elec-

tronic states or for revealing relative electronic–vibrational (e.g., exciton–phonon) couplings.

The GAMERS signal is formally fifth-order in the excitation pulse electric fields; however it can be instructive to think of it as a third-order process starting from an initial coherence rather than a population. This is justified because the interactions of the resonant and nonresonant pulses are physically distinct, with the former operating according to the dipole-moment operator, whereas the latter is through the electronic polarizability. The strength of these interactions may be quite different depending also on the field strengths of the resonant and nonresonant pulses, so that fifth-order perturbation theory may not directly apply. The nonresonant pulse is typically red-shifted with regard to the $S_0 \rightarrow S_1$ transition, so that one may avoid generating any excited-state population during the first period, T_0 . To first-order in perturbation theory, the density matrix in the interaction representation after interaction with the field is given by

$$\tilde{\rho}_{\mu,\mu'}(t) = \rho_{\mu,\mu'}^{(\text{eq})} - \frac{i}{\hbar} \Delta \rho_{\mu,\mu'}^{(\text{eq})} \int_0^t dt' H'_{\mu,\mu'}(t') \exp(i\omega_{\mu,\mu'} t')$$

Note that the coherence depends on the intensity envelope, $H'(t)$, of the nonresonant pulse and requires that the pulse duration be shorter than the vibrational period, $(\omega_{\mu,\mu'})^{-1}$, as expected for an impulsive Raman process. It is important to understand the effects of resonant and nonresonant excitation because the selection rules for these two processes differ. Resonant excitation depends on the overlap between the ground- and excited-state wave functions (i.e., the Franck–Condon factors), whose magnitude depends on vibronic coupling, whereas nonresonant excitation depends on the derivative of the transition moments with respect to normal modes (or combinations of normal modes).

After the initial state is created, the remaining nonlinear response can be treated in an identical manner to that used for third-order photon-echo spectroscopies such as 2D ES.³⁴ It is instructive to describe the different pathways using a diagrammatic representation of the density matrix after each field interaction, as shown in Figure 1b. For a given measurement, many coherence pathways may be considered, including pathways with both positive (R_3/R_4) and negative (R_3^*/R_4^*) frequencies during T_0 . (Note, we are not considering excited-state absorption pathways in this analysis.) From a response theory point-of-view, this simply corresponds to interactions of the field with either the bra or ket of the initial density operator; both processes occur because the experiment does not enforce a specific time ordering between the interactions with pulses 0 and 0', each of which contains both positive and negative frequencies in their real-valued electric fields. Fortunately, the signals corresponding to these positive and negative frequency coherences are easily distinguished because they appear in different quadrants of the multidimensional spectra. After a coherence is generated in the ground electronic state, it evolves for some time, T_0 , thereby encoding vibrational frequencies that are excited through the electronic polarizability operator. Owing to selection rules and depending on the detuning of the nonresonant pulse with respect to the lowest electronic state, only a small subset of the possible vibrational modes is typically excited. The third field–matter interaction is denoted by a dashed line because the signal is measured in a specific phase-matched direction, as discussed below, although, in principle, all possible fifth-order phase-matched directions may be measured, each encompassing a

different set of coherence pathways. (It is important to note that for any given excitation beam geometry, fifth-order signals may be generated in as many as $2^5 = 32$ different directions, many of which are either too weak to detect due to poor phase-matching or overlap with stronger lower-order signals, making signal isolation difficult.) The fourth interaction may occur on either the bra or ket side of the density operator, where the latter corresponds to R_3 and R_3^* , whereas the former corresponds to R_4 or R_4^* . The ambiguity of many early 2D ES experiments that report on beating signals during the time period, T , is, in fact, a direct result of the difficulty in distinguishing spectrally between the R_3 (R_3^*) and R_4 (R_4^*) pathways. Both generate coherences, with the difference being that the former consists of electronically excited states, whereas the latter is confined to the ground state. Clearly, when it comes to energy transfer, this distinction is critical.¹⁷ Finally, the last interaction creates a second SQC that radiates the signal during t . A key advantage of GAMERS, then, is that the SQC generated during T_0 must be on the ground state, whereas during the period T , coherences may be on either electronic surface. Therefore, after taking careful account of differences caused by selection rules, the examination of correlations between the two SQCs allows for the determination of the origin of coherence signals, assuming that there are resolvable shifts in energy (or lifetimes) caused by differences in the ground- and excited-state potential surfaces (see Figure 2). This is not the case for lower-order methods, where no such ground-state reference exists.

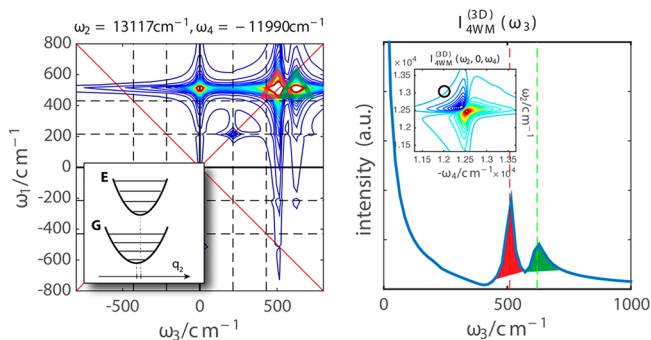


Figure 2. Left: Simulated 2DBS spectrum (i.e., 2D Raman spectrum extracted from a (ω_2, ω_4) point in the 4D GAMERS spectrum) showing a cross peak (green triangle) caused by slight differences in vibrational frequencies on the ground electronic potential versus excited electronic potential. Right: In a 1D beating spectrum constructed from a (ω_2, ω_4) point (black circle) in the 2D ES spectrum, both modes show up, but it is not possible to assign to either the ground or the excited state.

The combined use of resonant and nonresonant excitation makes GAMERS sensitive to nontrivial effects such as anharmonic coupling and electron–vibrational coupling while also avoiding the cascades that plagued fully nonresonant experiments. These advantages allow GAMERS to be applied to dilute solutions, unlike fully nonresonant experiments, which typically require pure solutions. Recently, Moran et al. demonstrated a fully resonant 6WM experiment,^{35,36} which also avoids the cascade problem but is only sensitive to anharmonicity through subtle changes in relative peak intensities. A particularly powerful feature of GAMERS, where there are two electronic and two vibrational frequency dimensions, is that different slices through the 4D spectrum reveal weak interactions that are, oftentimes, hidden in lower dimensionality projections. These include off-diagonal anhar-

monic couplings between vibrations, which lead to combination modes in the Raman spectrum. However, these signals may be completely swamped by the much stronger fundamental modes. Furthermore, in complex systems with many vibrational modes, there is no unambiguous method to tell if a mode is a fundamental or combination band based on spectral analysis alone. In simulations of GAMERS spectra, we have shown that appropriate cuts through the SQC–ZQC spectrum do indeed reveal new features within the 4D spectrum that no longer overlap with the strong signals arising from the fundamental modes.³⁷ Further theoretical analysis of GAMERS is needed to understand how different physical effects are manifested in the spectrum under more realistic relaxation conditions.

3. GAMERS EXPERIMENT

As discussed above, GAMERS is a fifth-order nonlinear spectroscopy in which five excitation pulses stimulate an emitted six-wave mixing (6WM) signal field that varies as a function of the relative delays between pulses. The experimental implementation of GAMERS requires some special considerations because the signal is exceptionally weak (typically 10^3 times smaller than resonant 4WM). As with other multidimensional coherent spectroscopies, the amplitude and phase of the signal field are recorded using spectral interferometry³⁸ over a range of interpulse delays and are subsequently Fourier-transformed to generate a coherent 4D spectrum. The photon-echo signal (e.g., the R_3 and R_4 pathways) is measured in the phase-matched direction given by $\hat{k}_{6WM} = -\hat{k}_0 + \hat{k}_0' - \hat{k}_1 + \hat{k}_2 + \hat{k}_3$. Other competing signal pathways are rejected by spatial filtering and phase cycling, as discussed below.

Another special consideration is that given the high dimensionality of the GAMERS experiment, efficient sampling of the 4D time–frequency space is necessary to make the experiment tractable. A brute force acquisition in which all four dimensions are parametrically scanned and Fourier-transformed would require >100 years given the weak fifth-order signal. Even when using a spectrometer and array detector as with most pump–probe or 2D ES techniques, the acquisition time would be hundreds of days. Instead, we employ a spatial encoding scheme such that two dimensions of the GAMERS signal field are detected simultaneously by Fourier transform spectral interferometry using a spectrograph fitted with a 2D pixel array detector. By vertically tilting beam 1 relative to beam 2 and horizontally focusing all beams to a common vertical line in the sample using a cylindrical curved mirror, the full range of τ delays is spatially encoded in the sample. Imaging the signal field to the spectrograph entrance preserves the spatial encoding such that the τ dimension is resolved along the vertical dimension of a 2D pixel array detector. This method simultaneously records the complete τ and ω_i dependence of the signal with each individual laser shot, leaving only the two remaining T and T_0 dimensions to be sampled parametrically. This gradient method, known as GRAPES,^{8,30,39–41} has the additional benefit of increasing the throughput of the experiment by using more of the sample to generate the signal than with traditional point-by-point (PBP) sampling. With these multiplexing methods, it is possible to reduce the acquisition time to fewer than a few hours.

Initial GAMERS experiments^{27,28} utilized a four-beam geometry in which pulses 0 and 0' were collinear. In this case, the phase-matched direction for 6WM signal radiation coincided with the direction of the phase-matched 4WM signal $\hat{k}_{4WM} = -\hat{k}_1 + \hat{k}_2 + \hat{k}_3$. A disadvantage of this geometry is that the 4WM and 6WM signals cannot be isolated from one another by

spatial filtering and therefore cannot be detected independently. Detecting the overlapped signals simultaneously limits the dynamic range of the measurement because fluctuations in the much (~ 1000 times) stronger 4WM signal overwhelms the weak 6WM signal. A significant improvement in sensitivity was achieved by employing a fully noncollinear five-beam geometry in which the 6WM signal was emitted in a background-free direction.²⁹ An additional advantage of the fully noncollinear geometry is the ability to perform pseudo-phase cycling. Because the phase of the signal is proportional to the phase of the excitation pulses, the sign of the signal can be inverted by shifting the phase of pulse 0' by π . By subtracting the signal measured with a π phase shift applied to pulse 0' from the signal measured without a phase shift, most interfering signals (e.g., excitation pulse scatter, 4WM pathways) can be eliminated while enhancing the strength of the signal.

Because the details of data processing in GAMERS have been described elsewhere,²⁷ we will only briefly review the steps here. Starting from the spectral interferograms in their initial form $S(T_0, \tau, T, \lambda)$, the GAMERS data are first interpolated along the wavelength axis onto a grid of equally spaced frequency points $S(T_0, \tau, T, \omega_i)$ and then Fourier-filtered to isolate one of the two spectral interference terms. Phase corrections are applied to account for the angular tilt between beam 3 and the local oscillator; then, the data are Fourier-transformed along the τ dimension to generate $\hat{S}(T_0, \omega_\tau, T, \omega_i)$, which represents the complex-valued 2D electronic spectra as a function of time delays T_0 and T . The next step is to remove the incoherent population relaxation dynamics along the T_0 and T dimensions, leaving only the oscillatory signals. This is accomplished by fitting the data to a model composed of a sum of exponential functions. The remaining coherent components are then Fourier-transformed along T_0 and T to form the 4D spectrum $\hat{S}(\omega_{T_0}, \omega_\tau, \omega_T, \omega_i)$.

Modeling of population dynamics is a critical part of generating GAMERS spectra because the accurate removal of the nonoscillatory background is required to avoid introducing distortions into the resulting spectrum. Rather than fitting to simple exponential decays, it is important to model the oscillatory and nonoscillatory components of the signal simultaneously to prevent low-frequency oscillations from biasing the decay time constants. One approach that was used in prior studies^{27,29} was to independently model the signal transient $\hat{S}(T)$ at each $(T_0, \omega_\tau, \omega_i)$ point in the data set using a sum of complex exponentials. Although simple and sufficient for many cases, this model does not take advantage of the commonality in dynamics across the $(T_0, \omega_\tau, \omega_i)$ dimensions and therefore overfits the data. An improved approach has been developed⁴² that models the dynamics (oscillatory and non-oscillatory) globally using a common set of time constants for all (ω_τ, ω_i) points (for the case of 3D GAMER spectra) or all $(T_0, \omega_\tau, \omega_i)$ points (for the case of 4D GAMER spectra). For a 3D GAMER spectrum, this model takes the form

$$\sum_{i=1}^n A_i(\omega_\tau, \omega_i) \exp(\hat{s}_i T)$$

where i indexes over n exponential functions, $A_i(\omega_\tau, \omega_i)$ are amplitudes, and \hat{s}_i are parameters defining the frequency $\omega_i = \text{Im}(\hat{s}_i)$ and decay rate $k_i = \text{Re}(\hat{s}_i)$ of the exponential functions. Once fit to the data, the components of the model corresponding to exponential population dynamics are identified and then subtracted from the data to leave only the

oscillatory part. In addition to being used for background subtraction, global analysis yields "oscillation maps", given by $A_i(\omega_\tau, \omega_i)$, that denote which parts of the electronic spectrum exhibit the oscillation frequency, ω_i .

4. 3D GAMERS: EXCITON-PHONON COUPLING IN CDSE QDS

In semiconductor nanomaterials, coupling between excitons and phonons dictates the relaxation dynamics of hot excitons. Phonons serve as a thermal bath into which excitons transfer their excess energy, facilitating transitions between excitonic states as they relax to the band edge. Consequently, an understanding of exciton-phonon coupling is critical for identifying and eliminating energy-loss pathways when designing efficient light-harvesting devices.

A significant challenge in studying exciton-phonon coupling is the ability to simultaneously resolve electronic and vibrational degrees of freedom. One approach is to use vibrationally resolved emission spectroscopy to estimate Huang-Rhys parameters. However, because of the high degree of electronic inhomogeneity, even in monodisperse nanoparticle samples, it is necessary to use single-particle methods at cryogenic temperatures to adequately resolve the vibrational progression. This route therefore relinquishes the advantage of ensemble-averaging and introduces selection bias and repetitive excitation issues. In addition, the properties of QDs may be strongly dependent on interactions at the particle surface, rendering tenuous comparisons of measurements in solid-state samples to solution properties. An alternative approach is to use resonance Raman scattering (RRS) to estimate exciton-phonon coupling.⁴³ Unfortunately, the results of this method are difficult to interpret because the Raman intensity of each mode is dependent on all other modes and is influenced by multiple electronic transitions.⁴⁴ Here we describe recent advances in applying GAMERS to probe exciton-phonon coupling in CdSe QDs.

A subset of the full 4D GAMER spectrum can be acquired by setting either T_0 to a fixed delay and then scanning the T delay or vice versa. This process yields a 3D GAMER spectrum and is useful in cases where adequately sampling a 2D space with sufficient signal-to-noise ratio is challenging. Initial GAMERS experiments on CdSe QDs by Spencer et al.²⁹ employed this approach to study how the ground state and excitonic states of QDs couple differently to phonons. The resulting "T-scan" GAMER spectrum resolved signatures from multiple excitonic states, which is in stark contrast with the broad and featureless 2DFT electronic spectrum. In addition, the 3D spectrum suggested that there is distinct coupling of the ground state and the first excitonic state (X_1) to the LO phonon mode at 25.8 meV.

Here we present a refinement of the GAMERS results in CdSe QDs by applying a global analysis method (see Section 3) to generate oscillation maps as well as 3D GAMERS spectra. Oscillation maps for the LO phonon modes, depicted in Figure 3a, agree qualitatively with the corresponding 2DBM spectra generated using the Fourier transform (figure 2 of ref 29). However, the global analysis oscillation maps exhibit increased signal-to-noise ratio thanks to improved exponential background subtraction and the averaging effect implicit in an underdetermined model. In addition, global analysis has been utilized to remove population dynamics prior to Fourier transforming along the T dimension when generating a 3D GAMER spectrum, as in Figure 3b.

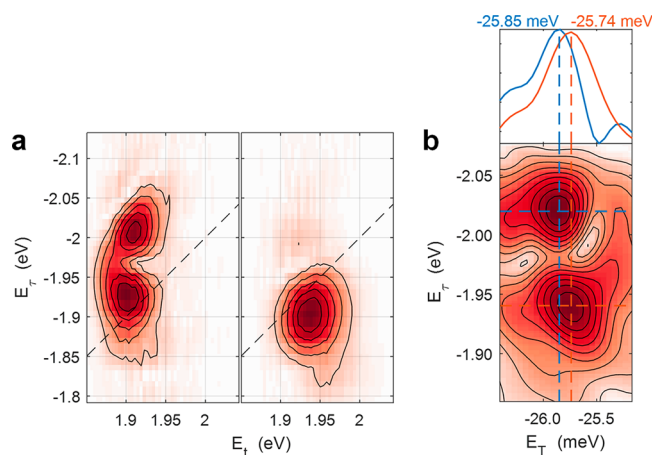


Figure 3. Global analysis of 3D GAMERS measurements in CdSe QDs. (a) Oscillation maps for the $\omega_T = -25.8$ meV (left panel) and $\omega_T = +25.8$ meV (right panel) LO modes show distinct excitonic-state-dependent coupling. (b) Slice of the GAMER spectrum at $E_t = 1.91$ eV reveals a $110 \mu\text{eV}$ difference between the LO phonons coupled to the X_1 state versus the ground state.

These results also highlight how dispersing the signal across multiple coupled dimensions affords GAMERS a high degree of coherence pathway specificity. Because the coherence frequency is resolved along all three dimensions, each peak in the GAMER spectrum can be attributed to a unique coherence pathway. This capability is critical for resolving differences in signals that otherwise overlap in lower dimensional spectra. For example, in Figure 3b, a slice of the spectrum taken at the center of the X_1 transition along the detection axis ($E_t \equiv \hbar\omega_t = 1.91$ eV) contains two distinct LO phonon peaks: one at the excitation energy of the X_1 transition and one at the excitation energy of the X_2 transition. Interestingly, these two peaks are offset from one another along $\hbar\omega_T$ by $110 \mu\text{eV}$, which is consistent with softening of the LO phonon mode in the X_1 state relative to the ground state. This implies that the LO phonon is dependent on the carrier distribution, which is known to differ between the ground and X_1 and X_2 exciton states. This supports the notion that coupling to LO phonons occurs by means of the Fröhlich mechanism, in which the electric field caused by the quantized electron and hole wave functions couples to the oscillating dipole of the optical phonon. Unpublished work⁵⁴ from our group on the same system further suggests that the acoustic phonons exhibit very different couplings to each excitonic state, which has important implications for the rates of exciton dephasing, as manifested by the homogeneous part of the absorption line width. The ability to measure such small effects in colloidal solutions at room temperature and in the presence of significant polydispersity suggests that GAMERS is a powerful method to extract details of the electronic and vibrational structure of semiconductor nanocrystals that are typically obscured by lower-order or lower-dimensionality methods.

5. 4D GAMERS AND RADIAL SAMPLING

One significant advantage of sampling the full 4D GAMERS space is the addition of vibrational–vibrational coupling information. 2D Raman spectra extracted from the GAMER spectrum directly map interactions between vibrations through the appearance of off-diagonal cross-peaks connecting modes with different frequencies. Furthermore, inspection of the 2DBM spectrum for a given vibrational mode not only reveals

which electronic states are coupled to this nuclear degree of freedom but also indicates if the vibration is involved in coupling different electronic states to one another.

The quantum-coherence selective properties of 4D GAMERS spectra have been demonstrated by Spencer et al.²⁷ in the tricyanocyanine dye IR-140. The 2DBM spectra of IR-140 in figure 4 of ref 27 illustrate the correlation between electronic and vibrational degrees of freedom, with shifts of the electronic features that are proportional to the selected Raman frequency. Comparison with coherence pathways fully explains the observed shifts, including the distinct types of spectral shifts observed for positive and negative frequency vibrational coherences due to differences in accessible pathways. However, measuring 4D GAMER spectra in this way is time-consuming, even with the speedup afforded by spatial multiplexing. For practical implementation of GAMERS when the scanning range of T and T_0 is greater than ~ 1 ps and the bandwidth of the excitation is $>500 \text{ cm}^{-1}$, a very different approach is necessary. If, for instance, the scanning range and Nyquist criteria require 256 points per dimensions, then traditional uniform sampling (US) of these dimensions requires 256^2 points, which may take many days or weeks of acquisition, especially if the nonlinear response is weak or there is significant scatter from the sample. Improvements to the sensitivity and data acquisition speed of GAMERS have come through the development of novel schemes for sampling the T_0 and T dimensions. The naïve US strategy, which was utilized in an initial study,²⁷ samples a rectangular grid in regular intervals in the (T_0, T) plane. This method is straightforward from the standpoint of Fourier processing but comes at the cost of n^2 scaling in sample points. A more efficient algorithm that takes advantage of the sparsity of the signal in the (ω_{T_0}, ω_T) plane involves sampling along radial lines at a range of angles through the origin of the (T_0, T) plane.³¹ Besides greatly reducing the number of points to sample, this method includes more points near $T = T_0 = 0$, where the signal is strongest. With radial sampling, the (ω_{T_0}, ω_T) dependence of the 6WM signal can be characterized with only n scaling in sample points. This method is related to the Radon transform methods utilized for reconstructing 2D tomograms from 1D projections in X-ray tomography and other imaging technologies. For spectroscopy, we utilize the projection-slice theorem, which states that the Fourier transform of a slice through the (T_0, T) plane contains the projection of the 6WM signal onto the same line in the (ω_{T_0}, ω_T) plane.⁴⁵ By recording projections of the signal from a few “perspectives” (i.e., slice angles), the full 2D shape of the signal can be unambiguously reconstructed, as shown in Figure 4. In practice, only about 8–32 slices are necessary depending on the complexity of the spectrum in the (ω_{T_0}, ω_T) plane, which corresponds to as little as a 3% sampling rate (i.e., the ratio of sampling compared to Nyquist). Note that unlike other methods of subsampling such as compressive sensing (CS),^{46,47} recovery of the spectrum is mathematically unique and does not require solving an underdetermined set of linear equations. It is therefore much more robust to noise and can achieve much lower sampling rates.

To generate the 4D GAMER spectrum from these slices, first, the population dynamics are removed using a multiexponential model; then, the remaining coherent components are Fourier-transformed to produce the frequency domain projections of the (ω_{T_0}, ω_T) plane. These projections are then used to reconstruct

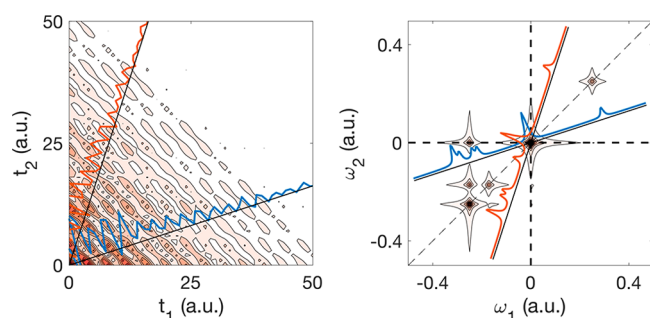


Figure 4. Left: Time-domain signal composed of coherence and population components. Right: Corresponding 2D Fourier transform (absolute value). Orange and blue slices show time traces and corresponding frequency spectra at select slices marked by a black solid line.

the (ω_{T_0}, ω_T) dimensions of the signal using one of many algorithms for the inverse Radon transform.⁴⁸ One of the simplest projection reconstruction (PR) methods is the filtered back-projection (FBP), which sums 2D “back-projections” of the various angled views of the (ω_{T_0}, ω_T) plane. The goal of FBP is to use the slice projections to reconstruct the full spectrum with as high fidelity as possible and, ideally, as few slices as possible. It is important to mention that due to causality, only the positive time quadrant is sampled in the experiment. Therefore, unlike conventional tomography (e.g., computed tomographic imaging), we do not have direct access to angles beyond 90° . In NMR, this issue has been addressed⁴⁹ by combining the results of different experiments with control over the phase of the pulses to extend the range to a full 180° . We have not applied this same principle to GAMERS, but, in principle, it should work given that the proper phase scheme is used.

When all of the projections are arranged in a matrix, the result is called a sinogram because a single point in frequency space will appear as a sine wave in projection space. There are multiple approaches to reconstructing the original image (i.e., 2D spectrum) from a sinogram, but the most straightforward is based on the inverse Radon transform. The continuous forward Radon transform is defined as

$$p(r, \theta) = \int \int_{-\infty}^{\infty} f(x, y) \delta(x \cos(\theta) + y \sin(\theta) - r) dx dy$$

where $f(x, y)$ is the image, and r and θ are the polar coordinates in the (ω_{T_0}, ω_T) plane. This expression is simply a statement that the signal is only sampled at points that lie on the line defined by the polar coordinates r and θ . The goal of reconstruction is to recover the original function, $f(x, y)$, with only knowledge of the projections, $p(r, \theta)$. The first step in reconstruction is to perform a back-projection, which is simply the reverse of the projection operation

$$f^{\text{BP}}(x, y) = \int_0^\pi p(x \cos(\theta) + y \sin(\theta), \theta) d\theta$$

It is straightforward to show that $f^{\text{BP}}(x, y) = r^{-1} * f(x, y)$, where $*$ denotes convolution. Therefore, the back-projection is a blurred representation of the original image, where the blurring function (i.e., point-spread function (PSF)) is r^{-1} . Because of this blurring, back-projection must be combined with a filtering step to recover the sharp features in the image

$$f(x, y) = \int_0^\pi p'(x \cos(\theta) + y \sin(\theta), \theta) d\theta$$

where

$$p'(r, \theta) = p(r, \theta) * b(r)$$

Known as a ramp filter, $b(r)$ is the Fourier transform of the function $|k|$, where k is the Fourier conjugate of r . Because the Fourier transform of a convolution is the product of the Fourier transforms of the original functions, many algorithms utilize the discrete Fourier transform (DFT) in reconstruction

$$\tilde{p}'(k, \theta) = \tilde{p}(k, \theta) |k|$$

where the tilde implies a DFT. The inverse Radon transform therefore requires two steps. The first is convolving the projection with the ramp filter, which can be done by Fourier-transforming the projection, multiplying by the ramp function, and then Fourier-transforming back. The second step is to use interpolation so that the image is evaluated at the desired points, usually on a rectangular grid.

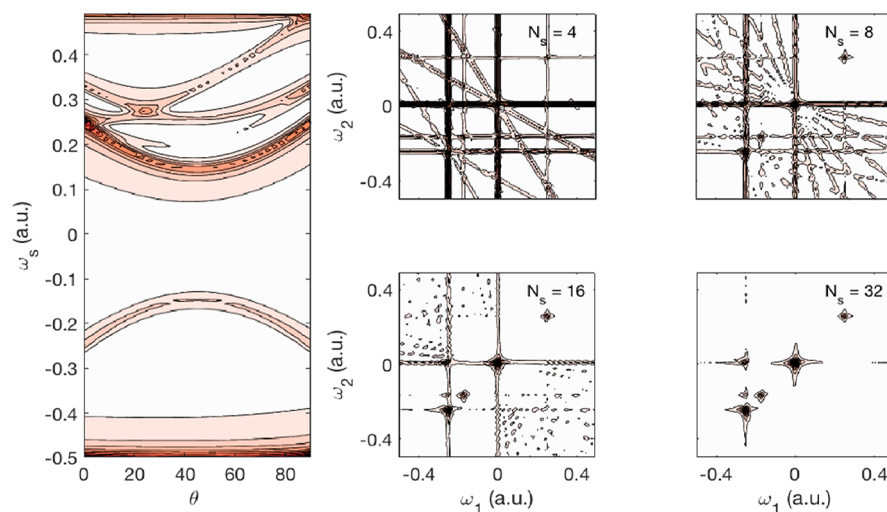


Figure 5. Left: Sinogram showing projections as a function of slice angle ($N_s = 32$). Right: Results of inverse Radon transform on simulated data with $N_s = 4, 8, 16,$ and 32 slices equally spaced between 0 and 90° .

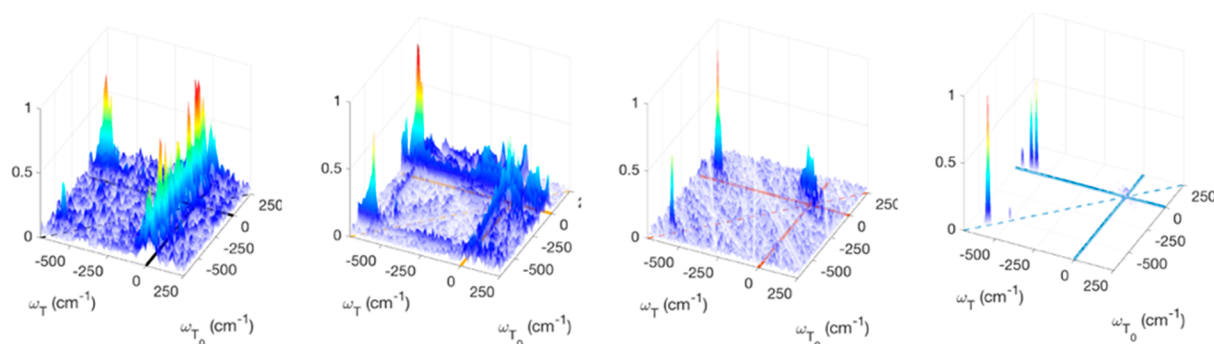


Figure 6. Comparison of experimental 2D Raman-like spectra (i.e., 2DBS spectra) at one point in the 2D SQC spectrum of Nile Blue reconstructed using various methods. From left to right: 2D FT, FBP with $N_s = 32$ slices, LV reconstruction, and hybrid LV with $k = 5$ bins.

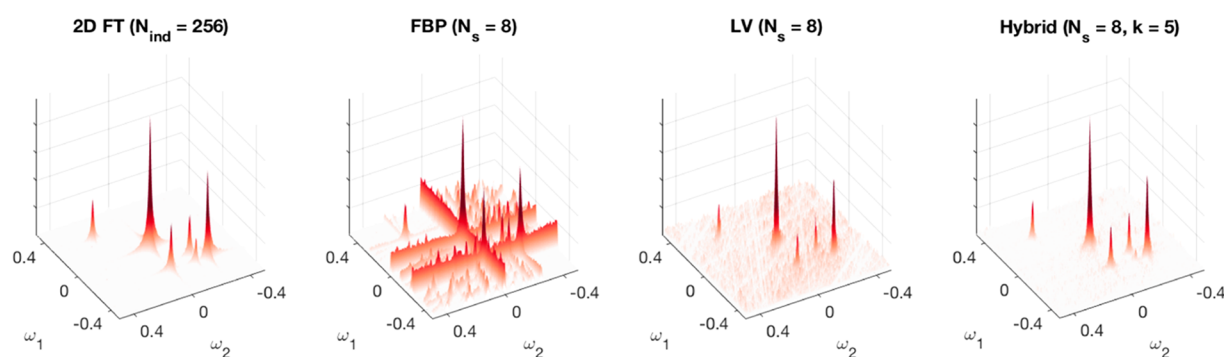


Figure 7. Comparison of simulated 2D Raman-like spectra (i.e., 2DBS spectra) reconstructed from the time-domain data shown in Figure 4 using various methods. From left to right: 2D FT, FBP with $N_s = 8$ slices showing strong ridge patterns, LV reconstruction eliminates most of the ridge structure, and hybrid LV with $k = 5$ bins completely eliminates ridges and recovers most of the spectral features including relative peak heights and peak positions.

Whereas this algorithm is stable and computationally efficient, it introduces ridge artifacts that appear as streaks across the spectrum from the back-projections. Unfortunately, the ridges form strong spectral features that can overwhelm weaker peaks, limiting the dynamic range of the recovered spectrum. These effects are easily seen in the simulations in Figure 5 for a small number of slices.

6. NONLINEAR RECONSTRUCTION: LOWEST-VALUE APPROACHES

As can be seen in Figure 6, FBP of experimental data results in artifacts that may appear as real features, which is concerning for spectroscopic applications. Whereas there is a marked improvement in signal-to-noise compared with Fourier transformation, the two methods are only formally equivalent as the slice number approaches infinity. In that case, FBP is simply the Fourier transform performed in polar coordinates. As an alternative, we have devised a means to eliminate the ridge structure using a method originating in NMR called lowest-value (LV) reconstruction,⁵⁰ which provides a significant sensitivity advantage when the number of slices is small. The key idea is to take advantage of the fact that true spectral features must appear in all projections. Therefore, by comparing the signals among each back-projection and taking the smallest value, one can replace ridge features at nonintersecting points with noise, whereas real signals where all of the back-projections intersect are replaced with the smallest values (which are equivalent among all of the back-projections to those within the noise). This replacement procedure is repeated for all points in the 2D vibrational spectrum. In GAMERS, as we discuss below, this

procedure is then repeated at each point in the 2D electronic spectrum. As can be seen in Figures 6 and 7, for both the experimental and simulated spectra, LV does indeed eliminate the ridge features. However, this artifact reduction procedure comes at the price that real signals may be inadvertently replaced by noise; unlike FBP, LV does not add the amplitude of the signals together, so the averaging effect of multiple slices (i.e., measurements) is lost.

The additive advantage of FBP and the artifact elimination of LV suggest that there should be a compromise between these two extremes. In a hybrid LV (HBLV) approach,⁵¹ the projections are grouped into k bins, so that among n projections there are $\binom{n}{k}$ different sets. For instance, if $n = 8$ slices are acquired and $k = 2$ bins are selected, then there would be 28 different pairs of projections. Each set is then averaged and back-projected (with a filter applied), and the back-projected spectra are compared as with LV. In the example above, 28 back-projections would be compared and, at each point, the lowest value among them selected. The advantage of the HBLV method is that by adjusting k , one can go from full FBP ($k = n$) to LV ($k = 1$). A larger bin size implies more buildup of signal amplitude while increasing the ridge artifacts. The real power of HBLV, however, is the statistical nature of the reconstruction. Even when using a relatively small number of slices, the number of sets can be very large: For instance, for $n = 16$ and $k = 8$, there are over 12 000 sets. For 32 slices and $k = 8$, there are over 10^7 different combinations. As a consequence, LV applied to such a large number of BPs results in nearly complete suppression of noise, which is uncorrelated across all of the different

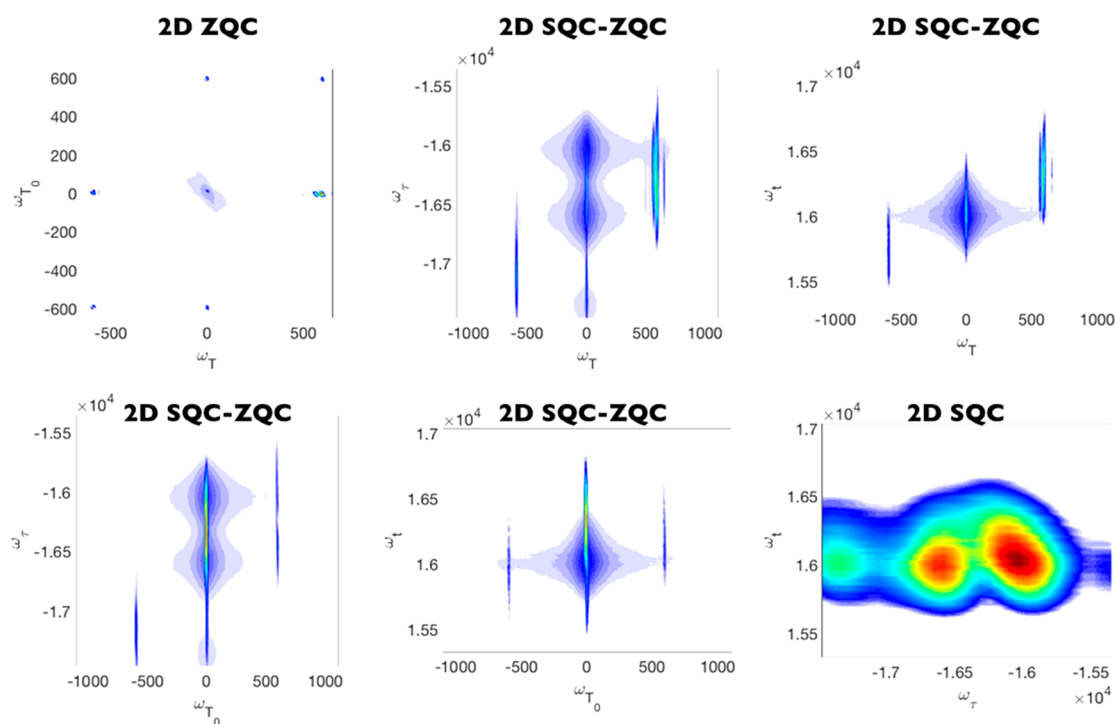


Figure 8. Six 2D projections of the HBLV-reconstructed 4D GAMER spectrum of Nile Blue include one 2D Raman-like spectrum (2D ZQC), one 2D electronic spectrum (2D SQC), and four mixed electronic–Raman spectra (2D SQC–ZQC).

projections. This is clearly evident in the simulation where HBLV recovers the ideal FT case, even with only 3% of the Nyquist sampling rate. In the experiment, the effect is much more dramatic because of the way noise enters into the signal. So-called indirect noise arises from the parametric sampling of delays,⁵² which strongly couples laser and sample fluctuations into the signal (i.e., multiplicative noise). As the scan time increases, the noise couples into the spectrum in a nonlinear fashion. Keeping the slice number small therefore has an oversized effect on suppressing noise. This can be seen in Figure 6 in the experimental 2D Raman spectrum reconstructed using HBLV as compared with 2D FT, despite HBLV using only a $\sim 16\%$ sampling rate.

Whereas HBLV reliably recovers peak locations and amplitudes, it does somewhat distort the peak shapes in the 2D Raman-like spectrum. As a nonlinear reconstruction method, one would predict that it would suppress the weak wings of the peak shapes relative to the maximum, as is observed when comparing to the 2D FT result in Figure 7. However, this does not significantly limit the interpretation of the GAMER spectrum because the vibrational peak shapes contain little more information than the vibrational dephasing rate, which is straightforward to extract from the time-domain slices if desired.

In general, PR methods,³¹ including HBLV, are most amenable to measuring relatively sparse spectra containing narrow resonances. As the spectrum becomes more congested (i.e., less sparse), due to either broader peak shapes or a greater density of peaks, peaks at different locations in the spectrum are more likely to overlap in the measured projections. In this case, peak shape distortions introduced by the PR method become more important, and a greater number of slice angles must be sampled to accurately reproduce the spectrum. Whereas this is not a concern for resonance Raman spectra, it may negate the advantage of PR methods relative to US when measuring other types of spectra.

7. HBLV-RECONSTRUCTED GAMERS SPECTRA OF NILE BLUE

To demonstrate the power of combining GAMERS with non-Fourier reconstruction to dramatically increase spectral resolution, we applied the approach to the well-studied fluorescent dye molecule, $C_{20}H_{20}N_3O^+$, also known as Nile blue (NB). A key challenge when studying the electronic structure of this system is the broad and featureless absorption and emission spectra, which mask much of the underlying vibronic structure. Whereas simple models have been employed to simulate these linear spectra, many of them rely on one or two displaced potential energy models, whereas in reality there are many dozens of coupled modes, as evidenced by extensive RRS studies.⁵³ A further issue is the separation of homogeneous from inhomogeneous broadening, which is critical for any quantitative analysis of its vibronic structure. However, RRS suffers from contamination by strong fluorescence background, which makes observing low-frequency modes ($<200\text{ cm}^{-1}$) particularly challenging. In addition, the analysis of RRS spectra is complicated when different modes overlap, which is often the case even for relatively “simple” organic molecules such as NB. Here we show that GAMERS can provide unprecedented spectral resolution beyond the homogeneous limit, revealing structure that is completely obscured in the absorption, emission, RRS, and 2D ES spectra. These results support our claim that GAMERS can provide ultrahigh spectral resolution of complex systems even at room temperature and in solution.

For NB, RRS spectroscopy identifies over 40 fundamental modes, although the majority of intensity below 1000 cm^{-1} is concentrated at 590 cm^{-1} , assigned to a ring-breathing mode. Note that in the absorption spectrum (figure 1 of ref 31), a barely perceptible shoulder is present that is $\sim 600\text{ cm}^{-1}$ from the main 0–0 peak, indicating that this mode is coupled to the $S_0 \rightarrow S_1$ electronic transition. Whereas modeling the absorption and emission spectra using all of the observed fundamental

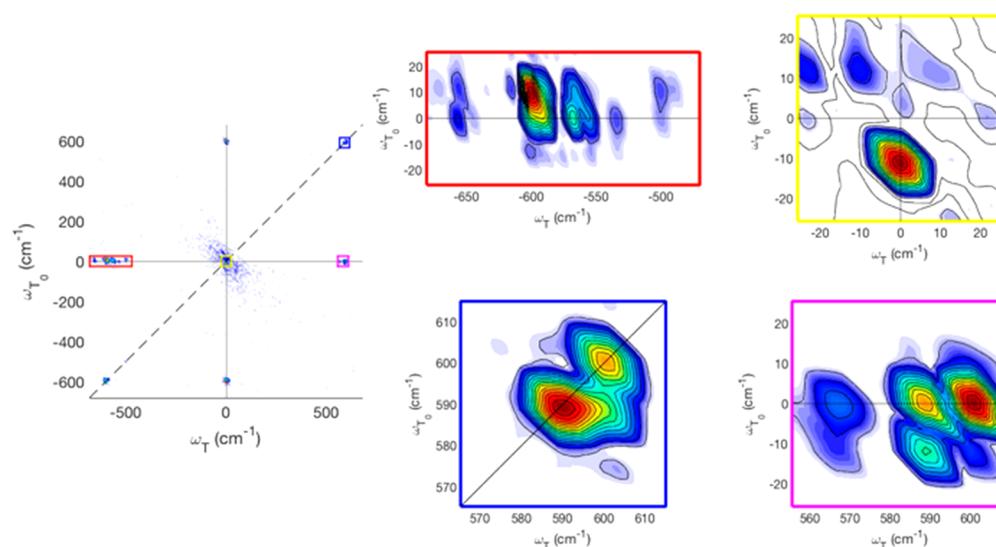


Figure 9. HBLV-reconstructed 2D ZQC (2D Raman-like) spectrum of NB and zoomed-in regions showing cross-peak features.

vibrational modes and their displacements, including appropriate damping parameters and inhomogeneous broadening, is possible, it does not necessarily represent a unique solution. Using GAMERS, however, we are able to select each vibrational mode and observe the 2DBS spectrum corresponding only to pathways that involve a particular ZQC energy along either ω_T , ω_{T_0} , or both. This leads to significantly better resolved spectra because it separates the contributions to the absorption from each vibrational mode, which circumvents the overfitting problem.

As shown in Figure 8, there are six different projections of the 4D GAMER spectrum of NB: 2D ZQC, 2D SQC, and four 2D SCQ–ZQC. The 2D Raman-like spectrum shows a pattern of sharp peaks at several diagonal and off-diagonal spectral locations. The most prominent are at $(\pm 590, \pm 590 \text{ cm}^{-1})$, and the corresponding off-diagonal positions are at $(\pm 590, 0 \text{ cm}^{-1})$. Note that the signal is primarily in the $(+/+)$ and $(-/-)$ quadrants. The reason for this is two-fold: (1) Theory predicts that in the absence of significant anharmonicity the signal is concentrated in these quadrants owing to the magnitude of the Franck–Condon factors, and (2) the signal is casual, meaning that only positive times are sampled, which causes streaks along the antidiagonal of the 2D Raman-like spectrum after HBLV reconstruction (see Figure 8). Whereas there are ways to manipulate the phase of the signal to acquire slices through both positive and, effectively, negative times, this was not done here. Whereas the 2D Raman-like spectrum appears to show only a small number of peaks, in contrast with RRS, which exhibits as many as 40 moderately intense peaks, this is really due to the difference in the dynamic range between the two experiments. In RRS, the peak amplitude is determined by the displacements and line-broadening functions (a reflection of the system–bath interactions). However, in GAMERS, there are effectively six field–matter interactions (if one counts the Raman interaction as two field–matter processes), which means that the relative peak strengths become highly nonlinear compared with RRS, which is linear in the field intensity. The result is that weak transitions are strongly suppressed, whereas strong transitions are amplified. Fortunately, HBLV is able to isolate even very weak spectral features, as small as 10^{-4} of the strongest coherence peaks. Such dynamic range is not achievable with

FT- or FBP-acquired spectra, where much stronger noise is manifested. Here we can observe many additional peaks that were not seen in either the FT or FBP spectra; in addition, we see an asymmetry between peaks along the T_0 and T axes, which is due to the difference in selection rules between the nonresonant and resonant excitation. The lack of cross peaks between different higher-frequency vibrational modes is a reflection of the lack of anharmonicity, although one does observe such features in the low-frequency region, as shown in Figure 9. These are presumably due to the highly delocalized low-frequency modes that couple to more localized high-frequency vibrations, although a more detailed theoretical analysis is needed to identify exactly which modes and by what mechanism cross peaks arise in the 2D Raman spectrum.

If we now examine the electronic–vibrational spectra (2D SQC–ZQC) in Figure 8, we may observe the coupling between each mode and each electronic state in the molecule. Because NB has only one low-lying electronic state, these maps simply reflect the degree of vibronic coupling. Again, we observe primarily the 590 cm^{-1} mode, although other vibronic modes are seen as well. Finally, we examine the 2D SQC spectrum, which is analogous to 2D ES with two significant differences: (1) All of the population dynamics have been removed, and (2) we primarily observe pathways that involve the most strongly coupled vibronic states, which for NB are dominated by the 590 cm^{-1} mode. This results in a 2D electronic spectrum that clearly shows the vibronic progression, which appeared as only a weak shoulder in the absorption spectrum. It is also worth pointing out that the line shape of these transitions clearly shows the extent of homogeneous versus inhomogeneous broadening, which is not possible to obtain directly by RRS, and is largely obscured even in 2D ES measurements.

8. CONCLUSIONS

GAMERS is a powerful method for disentangling the electronic and vibrational structure of complex chemical systems. The combination of resonance control along with the ability to disperse optical signals across four coupled frequency dimensions enables GAMERS to separate spectral features arising from distinct coherence pathways, thus exposing the fine detail beneath otherwise broad solution-phase line shapes. These capabilities have proven to be invaluable in discerning

hidden features within the vibronic structure of even well-studied systems, such as excitonic-state-dependent LO phonon frequencies in CdSe QDs.

A number of technical advances have been made to facilitate the use of GAMERS through improving its sensitivity and acquisition speed. The use of spatial–temporal encoding of delays in the sample exponentially reduces the acquisition time and is necessary to enable sampling of the large 4D time–frequency space. A radial sampling scheme was developed that further reduces the data acquisition requirements by about an order of magnitude and enables novel spectral reconstruction methods that greatly enhance the dynamic range. Reconstruction of GAMERS spectra using radially sampled data was tested using multiple methods, of which both FBP and HBLV were found to outperform Fourier transform reconstruction of a uniformly sampled grid.

In total, the experimental and data-processing advances that have been developed for GAMERS have significantly reduced the acquisition time while dramatically increasing the dynamic range and fidelity of the resulting spectra. These improvements have been critical in enabling GAMERS to access spectroscopically challenging chemical systems, thus broadening the reach of the technique to systems of fundamental interest, such as protein complexes and nanostructured devices, for which high-dimensional electronic–Raman spectroscopy can yield new insights into vibronic structure and dynamics on the femtosecond time scale.

AUTHOR INFORMATION

Corresponding Author

*E-mail: elharel@northwestern.edu.

ORCID

Austin P. Spencer: [0000-0003-4043-2062](https://orcid.org/0000-0003-4043-2062)

Elad Harel: [0000-0003-3007-0993](https://orcid.org/0000-0003-3007-0993)

Notes

The authors declare no competing financial interest.

Biographies



Austin P. Spencer researches coherent dynamics of coupled chromophores with Prof. Lin Chen at Northwestern University. Born in North Carolina, he attended the University of North Carolina Chapel Hill where he received a B.S. in chemistry. He then moved to the University of Colorado Boulder, where he earned his Ph.D. studying ultrafast carrier relaxation in quantum dots and developing a theory for modeling 2D Fourier transform spectra with Prof. David Jonas. Following graduate school, he moved to Chicago, where he worked with Prof. Elad Harel at Northwestern University to develop multidimensional spectroscopy methods and apply them to nanoma-

terials and light-harvesting protein complexes. A central theme of his research is to harness the coupling between electronic and vibrational modes as a probe of structure and dynamics in complex chemical systems.



Dr. William Hutson holds a Ph.D. in chemistry from Northwestern University and a B.S. in Chemistry from the University of Chicago. His graduate studies took place in the Harel Research group from 2013 to 2018, where he worked to implement high-order spectroscopic techniques (e.g., GAMERS). He currently works as an Instrument Engineer at TERA-print, LLC, a nanofabrication company started by Northwestern University Professor Chad Mirkin. His research interests include nonlinear spectroscopy of nanomaterials, optics engineering, and optical nanolithography.



Elad Harel was born in Israel but grew up in the Midwest. He obtained his B.A. and B.S. in mathematics and chemical physics, respectively, at the University of California, San Diego. In 2008, he obtained his Ph.D. under the supervision of Alexander Pines at the University of California, Berkeley, working on the development of new methods in NMR and MRI. He then left the field of magnetic resonance and started working on nonlinear spectroscopy during his postdoctoral work with Gregory Engel at the University of Chicago. There, he applied ideas in NMR and MRI to multidimensional coherent optical spectroscopy, where he invented the gradient-assisted photon-echo spectroscopy (GRAPES) method. These method advancements enabled new discoveries about the role of coherences in light-harvesting complexes and quantum dots. Since 2011, he has been an Assistant Professor at the Department of Chemistry at Northwestern University. His laboratory focuses on using high-order and high-dimensionality spectroscopy and imaging methods to study the role of the environment on carriers in a wide variety of systems from semiconductor nanocrystals, singlet-fission materials, organic molecules, organic–inorganic hybrid semiconductors, and photosynthetic complexes.

ACKNOWLEDGMENTS

This work was supported by the Office of Naval Research (N00014-16-1-2715-P00001), and the Packard Foundation (2013-39272) in part.

REFERENCES

- (1) Jonas, D. M. Vibrational and Nonadiabatic Coherence in 2D Electronic Spectroscopy, the Jahn–Teller Effect, and Energy Transfer. *Annu. Rev. Phys. Chem.* **2018**, *69*, 327–352.
- (2) Tempelaar, R.; Reichman, D. R. Vibronic Exciton Theory of Singlet Fission. III. How Vibronic Coupling and Thermodynamics Promote Rapid Triplet Generation in Pentacene Crystals. *J. Chem. Phys.* **2018**, *148*, 244701.
- (3) Spoor, F. C. M.; Tomic, S.; Houtepen, A. J.; Siebbeles, L. D. A. Broadband Cooling Spectra of Hot Electrons and Holes in PbSe Quantum Dots. *ACS Nano* **2017**, *11*, 6286–6294.
- (4) Dingley, A. J.; Pascal, S. M. *Biomolecular NMR Spectroscopy*; IOS Press: Washington, DC, 2011.
- (5) Gladden, L. Magnetic Resonance: Ongoing and Future Role in Chemical Engineering Research. *AIChE J.* **2003**, *49*, 2–9.
- (6) Ernst, R. R.; Bodenhausen, G.; Wokaun, A. *Principles of Nuclear Magnetic Resonance in One and Two Dimensions*; Clarendon Press: Oxford, U.K., 1988.
- (7) Jeener, J.; Meier, B. H.; Bachmann, P.; Ernst, R. R. Investigation of Exchange Processes by Two-Dimensional NMR Spectroscopy. *J. Chem. Phys.* **1979**, *71*, 4546–4553.
- (8) Harel, E.; Long, P. D.; Engel, G. S. Single-Shot Ultrabroadband Two-Dimensional Electronic Spectroscopy of the Light-Harvesting Complex LH2. *Opt. Lett.* **2011**, *36*, 1665–7.
- (9) Panitchayangkoon, G.; Hayes, D.; Fransted, K.; Caram, J.; Harel, E.; Wen, J.; Blankenship, R.; Engel, G. Long-Lived Quantum Coherence in Photosynthetic Complexes at Physiological Temperature. *Proc. Natl. Acad. Sci. U. S. A.* **2010**, *107*, 12766–12770.
- (10) Collini, E.; Wong, C. Y.; Wilk, K. E.; Curmi, P. M. G.; Brumer, P.; Scholes, G. D. Coherently Wired Light-Harvesting in Photosynthetic Marine Algae at Ambient Temperature. *Nature* **2010**, *463*, 644–647.
- (11) Zheng, J.; Fayer, M. D. Solute-Solvent Complex Kinetics and Thermodynamics Probed by 2D-IR Vibrational Echo Chemical Exchange Spectroscopy. *J. Phys. Chem. B* **2008**, *112*, 10221–10227.
- (12) Scholes, G. D.; Wong, C. Y. Biexcitonic Fine Structure of CdSe Nanocrystals Probed by Polarization-Dependent Two-Dimensional Photon Echo Spectroscopy. *J. Phys. Chem. A* **2011**, *115*, 3797–3806.
- (13) Velizhanin, K.; Piryatinski, A. Probing Interband Coulomb Interactions in Semiconductor Nanostructures with 2D Double-Quantum Coherence Spectroscopy. *J. Phys. Chem. B* **2011**, *115*, 5372–5382.
- (14) Bakulin, A. A.; Morgan, S. E.; Kehoe, T. B.; Wilson, M. W. B.; Chin, A. W.; Zigmantas, D.; Egorova, D.; Rao, A. Real-Time Observation of Multiexcitonic States in Ultrafast Singlet Fission Using Coherent 2D Electronic Spectroscopy. *Nat. Chem.* **2016**, *8*, 16–23.
- (15) Woys, A. M.; Lin, Y.-S.; Reddy, A. S.; Xiong, W.; de Pablo, J. J.; Skinner, J. L.; Zanni, M. T. 2D IR Line Shapes Probe Ovispirin Peptide Conformation and Depth in Lipid Bilayers. *J. Am. Chem. Soc.* **2010**, *132*, 2832–2838.
- (16) Tiwari, V.; Peters, W. K.; Jonas, D. M. Electronic Resonance with Anticorrelated Pigment Vibrations Drives Photosynthetic Energy Transfer Outside the Adiabatic Framework. *Proc. Natl. Acad. Sci. U. S. A.* **2013**, *110*, 1203–1208.
- (17) Tempelaar, R.; Jansen, T. L. C.; Knoester, J. Vibrational Beatings Conceal Evidence of Electronic Coherence in the FMO Light-Harvesting Complex. *J. Phys. Chem. B* **2014**, *118*, 12865–12872.
- (18) Engel, G.; Calhoun, T.; Read, E.; Ahn, T.; Mancal, T.; Cheng, Y.; Blankenship, R.; Fleming, G. Evidence for Wavelike Energy Transfer Through Quantum Coherence in Photosynthetic Systems. *Nature* **2007**, *446*, 782–786.
- (19) Hamm, P.; Zanni, M. T. *Concepts and Methods of 2D Infrared Spectroscopy*; Cambridge University Press: Cambridge, U.K., 2011.
- (20) Wilson, K. C.; Lyons, B.; Mehlenbacher, R.; Sabatini, R.; McCamant, D. W. Two-Dimensional Femtosecond Stimulated Raman Spectroscopy: Observation of Cascading Raman Signals in Acetonitrile. *J. Chem. Phys.* **2009**, *131*, 214502.
- (21) Kaufman, L. J.; Blank, D. A.; Fleming, G. R. Polarization Selectivity in Fifth-Order Electronically Nonresonant Raman Scattering from CS₂. *J. Chem. Phys.* **2001**, *114*, 2312–2331.
- (22) Blank, D. A.; Kaufman, L. J.; Fleming, G. R. Fifth-Order Two-Dimensional Raman Spectra of CS₂ Are Dominated by Third-Order Cascades. *J. Chem. Phys.* **1999**, *111*, 3105–3114.
- (23) Fidler, A.; Harel, E.; Engel, G. Dissecting Hidden Couplings Using Fifth-Order Three-Dimensional Electronic Spectroscopy. *J. Phys. Chem. Lett.* **2010**, *1*, 2876–2880.
- (24) Lynch, M. S.; Slenkamp, K. M.; Cheng, M.; Khalil, M. Coherent Fifth-Order Visible-Infrared Spectroscopies: Ultrafast Nonequilibrium Vibrational Dynamics in Solution. *J. Phys. Chem. A* **2012**, *116*, 7023–7032.
- (25) Zhang, Z. Y.; Wells, K. L.; Seidel, M. T.; Tan, H. S. Fifth-Order Three-Dimensional Electronic Spectroscopy Using a Pump-Probe Configuration. *J. Phys. Chem. B* **2013**, *117*, 15369–15385.
- (26) Brixner, T.; Mancal, T.; Stiopkin, I.; Fleming, G. Phase-Stabilized Two-Dimensional Electronic Spectroscopy. *J. Chem. Phys.* **2004**, *121*, 4221–4236.
- (27) Spencer, A. P.; Hutson, W. O.; Harel, E. Quantum Coherence Selective 2D Raman–2D Electronic Spectroscopy. *Nat. Commun.* **2017**, *8*, 14732.
- (28) Hutson, W. O.; Spencer, A. P.; Harel, E. Isolated Ground-State Vibrational Coherence Measured by Fifth-Order Single-Shot Two-Dimensional Electronic Spectroscopy. *J. Phys. Chem. Lett.* **2016**, *7*, 3636–3640.
- (29) Spencer, A. P.; Hutson, W. O.; Irgen-Giuro, S.; Harel, E. Exciton–Phonon Spectroscopy of Quantum Dots Below the Single-Particle Homogeneous Line Width. *J. Phys. Chem. Lett.* **2018**, *9*, 1503–1508.
- (30) Harel, E.; Fidler, A.; Engel, G. Real-Time Mapping of Electronic Structure with Single-Shot Two-Dimensional Electronic Spectroscopy. *Proc. Natl. Acad. Sci. U. S. A.* **2010**, *107*, 16444–16447.
- (31) Hutson, W. O.; Spencer, A. P.; Harel, E. Ultrafast Four-Dimensional Coherent Spectroscopy by Projection Reconstruction. *J. Phys. Chem. Lett.* **2018**, *9*, 1034–1040.
- (32) Engel, G. S.; Calhoun, T. R.; Read, E. L.; Ahn, T.-K.; Mančal, T.; Cheng, Y.-C.; Blankenship, R. E.; Fleming, G. R. Evidence for Wavelike Energy Transfer Through Quantum Coherence in Photosynthetic Systems. *Nature* **2007**, *446*, 782–786.
- (33) Gellen, T. A.; Lem, J.; Turner, D. B. Probing Homogeneous Line Broadening in CdSe Nanocrystals Using Multidimensional Electronic Spectroscopy. *Nano Lett.* **2017**, *17*, 2809–2815.
- (34) Mukamel, S. *Principles of Nonlinear Optical Spectroscopy*; Oxford University Press: New York, 1995.
- (35) Molesky, B. P.; Guo, Z. K.; Cheshire, T. P.; Moran, A. M. Two-Dimensional Resonance Raman Spectroscopy of Oxygen- and Water-Ligated Myoglobins. *J. Chem. Phys.* **2016**, *145*, 034203.
- (36) Molesky, B. P.; Guo, Z. K.; Cheshire, T. P.; Moran, A. M. Perspective: Two-Dimensional Resonance Raman Spectroscopy. *J. Chem. Phys.* **2016**, *145*, 180901.
- (37) Harel, E. Four-Dimensional Coherent Electronic Raman Spectroscopy. *J. Chem. Phys.* **2017**, *146*, 154201.
- (38) Lepetit, L.; Cheriaux, G.; Joffe, M. Linear Techniques of Phase Measurement by Femtosecond Spectral Interferometry for Applications in Spectroscopy. *J. Opt. Soc. Am. B* **1995**, *12*, 2467–2474.
- (39) Spencer, A.; Spokoyny, B.; Harel, E. Enhanced-Resolution Single-Shot 2DFT Spectroscopy by Spatial Spectral Interferometry. *J. Phys. Chem. Lett.* **2015**, *6*, 945.
- (40) Spokoyny, B.; Harel, E. Mapping the Vibronic Structure of a Molecule by Few-Cycle Continuum Two-Dimensional Spectroscopy in a Single Pulse. *J. Phys. Chem. Lett.* **2014**, *5*, 2808–2814.
- (41) Harel, E.; Fidler, A.; Engel, G. Single-Shot Gradient-Assisted Photon Echo Electronic Spectroscopy. *J. Phys. Chem. A* **2011**, *115*, 3787–3796.

(42) Volpato, A.; Bolzonello, L.; Meneghin, E.; Collini, E. Global Analysis of Coherence and Population Dynamics in 2D Electronic Spectroscopy. *Opt. Express* **2016**, *24*, 24773–24785.

(43) Gong, K.; Kelley, D. F.; Kelley, A. M. Nonuniform Excitonic Charge Distribution Enhances Exciton-Phonon Coupling in ZnSe/CdSe Alloyed Quantum Dots. *J. Phys. Chem. Lett.* **2017**, *8*, 626–630.

(44) Kelley, A. M. Electron–Phonon Coupling in CdSe Nanocrystals. *J. Phys. Chem. Lett.* **2010**, *1*, 1296–1300.

(45) Bracewell, R. N. *The Fourier Transform and Its Applications*, 3rd ed.; McGraw Hill: Boston, 2000.

(46) Spencer, A. P.; Spokoyny, B.; Ray, S.; Sarvari, F.; Harel, E. Mapping Multidimensional Electronic Structure and Ultrafast Dynamics with Single-Element Detection and Compressive Sensing. *Nat. Commun.* **2016**, *7*, 10434.

(47) Dunbar, J. A.; Osborne, D. G.; Anna, J. M.; Kubarych, K. J. Accelerated 2D-IR Using Compressed Sensing. *J. Phys. Chem. Lett.* **2013**, *4*, 2489–2492.

(48) Mersereau, R. M.; Oppenheim, A. V. Digital Reconstruction of Multidimensional Signals from Their Projections. *Proc. IEEE* **1974**, *62*, 1319–1338.

(49) Kupce, E.; Freeman, R. Reconstruction of the Three-Dimensional NMR Spectrum of a Protein from a Set of Plane Projections. *J. Biomol. NMR* **2003**, *27*, 383–387.

(50) Ridge, C. D.; Mandelshtam, V. A. On Projection-Reconstruction NMR. *J. Biomol. NMR* **2009**, *43*, 151–159.

(51) Harel, E. Zooming in on Vibronic Structure by Lowest-Value Projection Reconstructed 4D Coherent Spectroscopy. *J. Chem. Phys.* **2018**, *148*, 194201.

(52) Granwehr, J. Multiplicative or T(1) Noise in NMR Spectroscopy. *Appl. Magn. Reson.* **2007**, *32*, 113–156.

(53) Lawless, M. K.; Mathies, R. A. Excited-State Structure and Electronic Dephasing Time of Nile Blue from Absolute Resonance Raman Intensities. *J. Chem. Phys.* **1992**, *96*, 8037–8045.

(54) Hutson, W. O.; Spencer, A. P.; Irgen-Gioro, S.; Harel, E. Exciton-State–Dependent Coupling to Acoustic Phonons in CdSe Quantum Dots. In preparation.